



Please cite the Published Version

Zhou, J , Freeman, CT and Holderbaum, W  (2025) Multiple-model iterative learning control with application to stroke rehabilitation. *Control Engineering Practice*, 154. 106134 ISSN 0967-0661

DOI: <https://doi.org/10.1016/j.conengprac.2024.106134>

Publisher: Elsevier

Version: Published Version

Downloaded from: <https://e-space.mmu.ac.uk/637039/>

Usage rights:  [Creative Commons: Attribution-Noncommercial-No Derivative Works 4.0](https://creativecommons.org/licenses/by-nc-nd/4.0/)

Additional Information: This is an open access article published in *Control Engineering Practice*, by Elsevier.

Enquiries:

If you have questions about this document, contact openresearch@mmu.ac.uk. Please include the URL of the record in e-space. If you believe that your, or a third party's rights have been compromised through this document please see our Take Down policy (available from <https://www.mmu.ac.uk/library/using-the-library/policies-and-guidelines>)



Multiple-model iterative learning control with application to stroke rehabilitation

Junlin Zhou^{a,*}, Christopher T. Freeman^a, William Holderbaum^b

^a School of Electronics and Computer Science, University of Southampton, University Road, Southampton, SO17 1BJ, UK

^b Department of Mathematics and Engineering, University of Reading, Whiteknights, Reading, Berkshire, RG6 6AH, UK

ARTICLE INFO

Keywords:

Iterative learning control
Multiple-model adaptive control
Robust stability
Functional electrical stimulation
Upper limb stroke rehabilitation

ABSTRACT

Model-based iterative learning control (ILC) algorithms achieve high accuracy but often exhibit poor robustness to model uncertainty, causing divergence and long-term instability as the number of trials increases. To address this, an estimation-based multiple-model switched ILC (EMMILC) approach is developed based on novel theorem results which guarantee stability if the true plant lies within a uncertainty space defined by the designer. Using gap metric analysis, EMMILC eliminates restrictive assumptions on the uncertainty structure assumed in existing multiple-model ILC methods. Our design framework minimises computational load while maximising tracking accuracy. Applied to a common rehabilitation scenario, EMMILC outperforms the standard ILC approaches that have been previously employed in this setting. This is confirmed by experimental tests with four participants where performance increased by 28%. EMMILC is the first model-based ILC framework that can guarantee high performance while not requiring any model identification or tuning, and paves the way for effective, home-based rehabilitation systems.

1. Introduction

Every year 12.2 million people suffer from their first stroke. Approximately 70% of survivors report impaired upper-limb function, and 40% are left with a permanent arm disability (Party, 2023). Fortunately, this lost movement can be recovered by intensive practice of functional tasks (Geller et al., 2023) which enables the brain to fuse new connections in the motor cortex that replace those lost by stroke. This ‘relearning’ is facilitated by haptic, proprioceptive and visual feedback during goal-orientated functional tasks. However, conventional therapy only promotes limited recovery for less severe impairment levels, and is increasingly unaffordable. There is therefore an urgent need for low-cost technology to provide intensive, goal-oriented task training (Ballester, Ward, Brander, et al., 2022).

Functional electrical stimulation (FES) comprises a sequence of electrical pulses that are applied using electrodes to artificially activate muscles. Recent UK National Clinical Guidelines for stroke (Party, 2023) strongly recommend using FES during daily practice of repeated arm movements. However, they highlight that current FES devices used in clinics and hospitals employ open-loop or triggered control (Kristensen, Busk, & Wienecke, 2022; Popović, 2014; Schearer et al., 2012; Wolf & Schearer, 2017). This is due to the need for simple, reliable and fast set-up, however it has resulted in slow and inaccurate upper-limb

movements which are not personalised to users and do not promote recovery (Anderson, 2004).

Meta-analyses confirm that FES systems used in clinical upper-limb studies are still overwhelmingly open-loop or triggered by electromyography (Kristensen et al., 2022). A small number of clinical studies have employed simple closed-loop feedback (leung Chan, Yu Tong, & kwan Chung, 2009; Hodkin et al., 2018; Pelton, van Vliet, & Hollands, 2012; Resquín, Cuesta Gómez et al., 2016), however their tracking accuracy is still relatively low, particularly due to the slow system response and onset of muscle fatigue. Controllers often require extensive tuning for each subject (Resquín, Gonzalez-Vargas et al., 2016; Wiarta, Arifin, Baki, Arrofiqi, Fatoni, & Watanabe, 2020) which is impractical in clinical practice due to time constraints and lack of expertise. Higher accuracy tracking has been achieved using model-based FES upper-limb control strategies, including model predictive (Westerveld, Schouten, Veltink, & van der Kooij, 2014; Wolf & Schearer, 2022), optimal (Sae, Freeman, & Yang, 2020), active disturbance rejection (Liu, Qin, Huo, & Wu, 2020), and sliding mode (Oliveira, Costa, Catunda, et al., 2017; Rouse, Parikh, Duenas, et al., 2016; Wu, Wang, Du, et al., 2017) control. To avoid the need for time-consuming identification, Razavian, Ghannadi, Mehrabi, et al. (2018), Tan, Shee, Kong, Guan, and Ang (2011), Wolf and Schearer (2019) and Wolf and Schearer (2018) use

* Corresponding author.

E-mail addresses: jz3c20@soton.ac.uk (J. Zhou), ctfl@soton.ac.uk (C.T. Freeman), w.holderbaum@reading.ac.uk (W. Holderbaum).

only partial model information, however this degraded tracking accuracy. Like all the above methods, a further drawback was their inability to adequately compensate for fatigue, spasticity and other physiological effects.

Adaptive FES model-based controllers have attempted to improve performance. A prominent example is multiple-model adaptive control (MMAC) (Brend, Freeman, & French, 2015) which defines a set of ‘candidate’ plant models, and a corresponding set of optimal controllers. A bank of Kalman filters are used to switch in the controller whose model best fits the observed plant data. An experimental evaluation with five subjects performing isometric elbow force tracking showed it improved accuracy by 22% compared with standard optimal control. Together with (Wolf, Hall, & Scheerer, 2020), this is the only model-based upper-limb controller tested in experiments with multiple subjects that induce prolonged muscle fatigue. There have been other significant advancements in robust upper-limb FES controllers, including switched designs to address electromechanical delays (Allen, Cousin, Rouse & Dixon, 2022; Sharma, Gregory, & Dixon, 2011), varying geometry of the upper-limb muscles (Allen, Stubbs, & Dixon, 2022), or co-activation of antagonistic muscles (Sun, Qiu, Iyer, Dicianno, & Sharma, 2023). However, they cannot provide guaranteed high performance tracking in the presence of arbitrarily large, unstructured model uncertainty. These approaches have been tested with unimpaired subjects. With one exception (Alibeji, Kirsch, Dicianno, & Sharma, 2017), they have not progressed to tests with neurologically impaired participants.

Iterative learning control (ILC) is one of the few model-based control schemes that have been applied to FES-based upper-limb control with impaired patients. It has shown its success in five clinical trials (Freeman, 2016) with more than 30 patients with stroke (Kutlu, Freeman, Hallewell, et al., 2016) or multiple sclerosis (Sampson et al., 2016). ILC is formulated for systems that repeat the same finite duration tracking task, and aims to capture the idiom that ‘practice makes perfect’. It updates the control input using information from previous attempts, which exactly matches the rehabilitation scenario. Early ILC algorithms did not use model information (Arimoto, Kawamura, & Miyazaki, 1984; Freeman, Lewin, & Rogers, 2005; Nahrstaedt, Schauer, Shalaby, Hesse, & Raisch, 2008), however the field rapidly expanded to leverage model-based updates in order to provide greater accuracy and convergence properties for wider system classes. Examples of the broad range of model-based ILC approaches are contained in Bristow, Tharayil, and Alleyne (2006), Owens (2016) and Rogers, Chu, Freeman, and Lewin (2023) and the references therein. An essential aspect of ILC that has been widely studied is long-term robust stability (Bradley, 2010; Freeman et al., 2005; Meng & Moore, 2017), which refers to the system’s ability to maintain stability after initial convergence, even in the presence of modelling errors. For example, Ratcliffe et al. (2005) showed that a common ILC update will diverge if a multiplicative model uncertainty has a phase angle greater than 90° in magnitude. Addressing long term stability is especially crucial in a rehabilitation setting to ensure that the intensive FES training remains effective, comfortable and safe over extended periods of use.

Several ILC schemes have been applied to FES based upper limb rehabilitation, with standard model-based updates proving most accurate. Tests with stroke participants showed they outperforming conventional model-based strategies by an order of magnitude (Freeman, 2016). Over the course of fifteen years, ILC has progressed from purely elbow extension to full arm reaching tasks (Kutlu et al., 2016) including hand and wrist motion via a 24 channel FES electrode array (Excell, Freeman, Meadmore, et al., 2013). Although accuracy has been high, the time needed for identification has become prohibitively long, and recent trials which avoided re-identification by reusing previous models yielded significantly degraded tracking accuracy (Kutlu et al., 2016).

To solve the above deficiencies, a new control approaches is needed that requires little or no model identification tests, but is capable of accurate tracking in the presence of substantial model uncertainty (e.g. fatigue, spasticity and electrode movement). ILC is an obvious

starting point given its pedigree in rehabilitation, and there already exist a range of robust ILC algorithms that may be suitable for application in rehabilitation. However, closer inspection reveals these have focused on highly structured parametric (Ahn, Moore, & Chen, 2005; Xu & Xu, 2013) or multiplicative/additive (Donkers, van de Wijdeven, & Bosgra, 2008; Freeman, Lewin et al., 2009; Owens, Freeman, & Chu, 2014) forms. Model predictive and simple adaptive strategies have also been embedded into the ILC framework to address time-iteration-dependent uncertainties. Unfortunately, their accuracy is subject to modelling error (Ma, Liu, Kong, & Lee, 2021) and relies on restrictive assumptions on the form of uncertainties (Zhang, Meng, & Cai, 2023). Methods that can be applied to more general uncertainties typically require substantial identification/training time, excessive tuning, or place additional structural assumptions (Lee, Lee, & Kim, 2000; Meng, 2019; Meng & Moore, 2017). A promising avenue are ILC approaches that update the model in order to better capture the plant dynamics. Li, Wang, and Liu (2014) and Li and Zhang (2010) used fuzzy neural networks to approximate multiple underlying nonlinear models and select the best one for ILC at every time sample. Longman, Peng, Kwon, et al. (2011) updated the model in between ILC trials using a standard model identification approach. This focused on linear systems, and only considered inverse ILC. It also did not provide any stability or robust performance guarantees. Instead of switching between different ILC updates, Zhu, Xu, Huang, et al. (2015) specified multiple linear models to capture unknown iteration-varying parameters, and designed a single ILC update using H_∞ tools which can stabilise all specified models. Similarly, Padmanabhan, Bhushan, Hebbar, et al. (2021) captured parametric uncertainty by producing multiple linear models, and designed ILC using a convex combination of all plants. Unfortunately, there is currently no switched multiple model framework that derives robust performance bounds for the most common ILC update structure when the plant model is subject to a general class of modelling uncertainty specified by the designer. Additionally, there is no principled multiple-model guidelines allowing the designer to systematically and efficiently generate the required plant models and associated ILC updates. In terms of application, none of the above approaches has been used in FES upper limb rehabilitation.

This paper develops a multiple-model ILC framework that addresses the above limitations. It is motivated by the previous multiple-model approach of Brend et al. (2015), which applied optimal control to stabilise the isometric elbow using FES. This was a direct application of theory developed in Buchstaller and French (2016a) and Buchstaller and French (2016b) which considered only regulation (i.e. maintaining the system states at zero). Despite this narrow remit, the MMAC theory is less conservative than competing multiple-model approaches since it derives bounds on the output that do not scale with the number of plant models. In addition, it permits a broader class of uncertainties through use of the gap metric, a powerful measure of plant mismatch. Our results in Freeman and French (2015) showed how the MMAC framework could be extended to address ILC through two major extensions: (1) MMAC operates from sample to sample, whereas ILC resets after each trial. We addressed this by packaging ILC as a single sample of a high dimension system, and (2) by modifying the operating point to extend the regulation problem to tracking. Both components are non-trivial, and require substantial extension of all components of the framework (i.e. the estimators, gap metric definitions, controller properties, and overall performance bounds). Unfortunately, the resulting EMMILC framework (Freeman & French, 2015) entailed intensive computational burden, limiting its practicality. It was only applied numerically to a simple problem. To solve these problems, we make the following contributions:

1. We propose the first multiple-model ILC framework that is both simple to apply in practice, and guarantees robust performance for general uncertainty classes. A key component is a new robust performance bound that defines the uncertainty space stabilised

by existing ILC laws. Another critical component is a novel design procedure that produces a candidate model set without requiring *any* further model identification. This set guarantees robust stability while transparently balancing computational load and tracking accuracy.

2. We describe the first experimental application of EMMILC, focusing on a clinically important rehabilitation problem. We show how a model set can be designed to capture the full range of physiological variation while imposing minimal computational load. Results confirm the practical efficacy of EMMILC and opens up the possibility of translating effective FES technology to patients' own homes for the first time.

We build on preliminary work in [Zhou, Freeman, and Holderbaum \(2023a\)](#) which applied EMMILC in simulation, but contained no performance bounds, identification procedures or experiments.

This paper is organised as follows: Section 2 gives an overview of ILC preliminaries and applies robust stability analysis. Section 3 introduces a multiple-model control framework together with a practical design procedure guaranteeing robust stability. Then, Section 4 defines a wrist model, and expands its identification to capture an uncertainty set. Section 5 applies the framework to rehabilitation and describes the associated hardware implementation. Results involving four healthy subjects are given in Section 6, including comparison with standard ILC to confirm its practical efficacy.

2. Problem statement

This section summarises the ILC framework and uses gap metric analysis to derive bounds on the maximum modelling error that may be tolerated while preserving stability.

2.1. ILC framework

ILC is applicable to systems that repeat the same finite duration tracking task. Each attempt is termed a trial, with index $k = 0, 1, 2, \dots$. Each trial runs over N samples, after which the plant is reset to the same initial condition $x_0 = 0$. The signals have a natural 2D structure, thus we denote $\tilde{u}_1(k, t)$, $\tilde{y}_1(k, t)$ to be the underlying input and output signals, and assume the discrete time state-space system dynamics

$$\begin{aligned} \tilde{x}(k, t+1) &= A_p \tilde{x}(k, t) + B_p \tilde{u}_1(k, t), \quad \tilde{x}(k, 0) = x_0 \\ \tilde{y}_1(k, t) &= C_p \tilde{x}(k, t) + D_p \tilde{u}_1(k, t), \quad t = 0, 1, \dots, N-1, \end{aligned} \quad (1)$$

where the state-space quartet $p = (A_p, B_p, C_p, D_p) \in \mathbb{R}^{p \times p} \times \mathbb{R}^{p \times m} \times \mathbb{R}^{n \times p} \times \mathbb{R}^{n \times m}$. The corresponding plant operator P_p , defines the mapping $\tilde{y}_1(k, \cdot) = P_p \tilde{u}_1(k, \cdot)$. The ILC objective is for $\tilde{y}_1(k, t)$ to track a fixed reference signal $y_{ref}(t)$ as the trials progress, i.e.

$$\lim_{k \rightarrow \infty} \tilde{y}_1(k, t) = y_{ref}(t), \quad t = 0, 1, 2, \dots, N-1. \quad (2)$$

ILC typically operates in the lifted (or supervector) framework, in which data is packaged from the k th trial as

$$\begin{aligned} u_1(k) &= (\tilde{u}_1(k, 0), \tilde{u}_1(k, 1), \tilde{u}_1(k, 2), \dots, \tilde{u}_1(k, N-1))^T \\ y_1(k) &= (\tilde{y}_1(k, 0), \tilde{y}_1(k, 1), \tilde{y}_1(k, 2), \dots, \tilde{y}_1(k, N-1))^T \\ y_{ref} &= [y_{ref}(0), y_{ref}(1), y_{ref}(2), \dots, y_{ref}(N-1)]^T \end{aligned} \quad (3)$$

and the lifted plant dynamics are then expressed as the map

$$y_1(k) = P_{\hat{p}} u_1(k), \quad (4)$$

where \hat{p} denotes the lifted realisation of plant p , with associated matrix operator $P_{\hat{p}} =$

$$\begin{bmatrix} D_p & 0 & \dots & 0 & 0 \\ C_p B_p & D_p & \dots & 0 & 0 \\ C_p A_p B_p & C_p B_p & \dots & 0 & 0 \\ \vdots & \vdots & \ddots & \vdots & \vdots \\ C_p A_p^{N-3} B_p & C_p A_p^{N-4} B_p & \dots & D_p & 0 \\ C_p A_p^{N-2} B_p & C_p A_p^{N-3} B_p & \dots & C_p B_p & D_p \end{bmatrix} \in \mathbb{R}^{mN \times nN}. \quad (5)$$

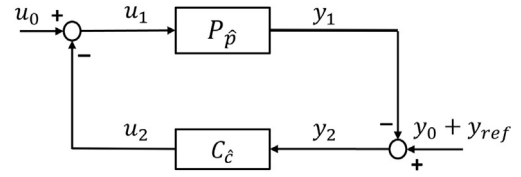


Fig. 1. Closed-loop system structure $[P_{\hat{p}}, C_{\hat{c}}]$.

As $P_{\hat{p}}$ describes a linear system, we can represent the lifted dynamics by a state space system in the lifted space with parameter $\hat{p} = (0, 0, 0, P_p) \in \mathbb{R}^{pN \times pN} \times \mathbb{R}^{pN \times mN} \times \mathbb{R}^{nN \times pN} \times \mathbb{R}^{nN \times mN}$. Each ILC trial can be regarded as a single sample of this high dimension lifted system. Given p we will denote the same plant dynamics in the lifted space as \hat{p} , with respective operators P_p and $P_{\hat{p}}$, where

$$P_{\hat{p}} : u_1 \mapsto y_1, \quad \tilde{y}_1(k, \cdot) = P_{\hat{p}} \tilde{u}_1(k, \cdot). \quad (6)$$

Since the lifted dynamics are expressed in a single variable (k), they fit in the standard closed loop structure of Fig. 1 where $w_i = (u_i, y_i)^T$ represents the plant input and output ($i = 1$), external disturbances ($i = 0$) and controller signals ($i = 2$). The reference y_{ref} appears as an external bias, so that the controller input y_2 is equal to the tracking error. A wide variety of ILC designs exist, see, for example, [Bristow et al. \(2006\)](#) for a review. The majority of ILC updates take a lifted form and therefore can be expressed by the lifted control operator $C_{\hat{c}}$. In particular, the most common ILC update algorithm is

$$u_2(k+1) = Q_{\hat{c}}(u_2(k) - L_{\hat{c}} y_2(k)), \quad (7)$$

where $Q_{\hat{c}} \in \mathbb{R}^{mN \times mN}$ is a robustness filter and $L_{\hat{c}} \in \mathbb{R}^{mN \times nN}$ is a learning operator. Signal y_2 is the measured tracking error, which, in the absence of disturbance, is $y_{ref} - y_1$. From (7), lifted operator $C_{\hat{c}}$ is a state-space system parameterised by $\hat{c} = (Q_{\hat{c}}, -Q_{\hat{c}} L_{\hat{c}}, I, 0) \in \mathbb{R}^{mN \times mN} \times \mathbb{R}^{mN \times nN} \times \mathbb{R}^{nN \times mN} \times \mathbb{R}^{mN \times nN}$.

The standard ILC convergence condition is

$$\sigma := \|Q_{\hat{c}}(I - L_{\hat{c}} P_{\hat{p}})\| < 1 \quad (8)$$

which, if there are no disturbances, i.e. $(u_0, y_0)^T = 0$, guarantees $y_1(k) \rightarrow (I - Q_{\hat{c}}(I - L_{\hat{c}} P_{\hat{p}}))^{-1} Q_{\hat{c}} L_{\hat{c}} P_{\hat{p}} y_{ref}$ as $k \rightarrow \infty$. In particular, if $Q_{\hat{c}} = I$, then tracking objective (2) holds. Note that $\|\cdot\|$ denotes the 2-norm throughout this paper.

2.2. ILC robust stability

This section derives a robust stability condition for the nominal ILC system $[P_{\hat{p}}, C_{\hat{c}}]$ which will be used in the later EMMILC design framework. This employs the gap metric, a well known measure characterising the distance between two systems ([Zames & El-sakkary, 1980](#)) that underpinned the EMMILC design framework of [Buchstaller and French \(2016a\)](#). Given two unlifted plant operators P_p, P_{p^*} , the gap metric between them is denoted $\delta(p, p^*)$. It was shown in [Bradley \(2010\)](#) that $\delta(p, p^*)$ is related to the corresponding lifted gap by

$$\delta(\hat{p}, \hat{p}^*) \leq \delta(p, p^*), \quad (9)$$

where \hat{p}, \hat{p}^* are the lifted forms of plants p, p^* . This relation is used in the next result which establishes a robust stability margin for ILC. This uses the following maps from external to internal signals for $[P_{\hat{p}}, C_{\hat{c}}]$, $[P_{\hat{p}^*}, C_{\hat{c}}]$ respectively

$$\Pi_{P_{\hat{p}}/C_{\hat{c}}} : (u_0, y_0)^T \mapsto (u_1, y_1)^T \quad (10)$$

$$\Pi_{P_{\hat{p}^*}/C_{\hat{c}}} : (u_0, y_0)^T \mapsto (u_1, y_1)^T. \quad (11)$$

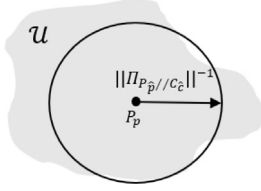


Fig. 2. Gap ball of plants stabilised by ILC update $C_{\hat{c}}$, with centre P_p , and radius $\|II_{P_p}/C_{\hat{c}}\|^{-1}$.

Theorem 1. Let P_p, P_{p^*} be systems of form (1) and $C_{\hat{c}}$ be an ILC design for P_p such that condition (8) holds. Then this ILC design also stabilises the true plant P_{p^*} provided

$$\delta(p, p^*) < \|II_{P_p}/C_{\hat{c}}\|^{-1}, \quad (12)$$

where the mapping

$$\|II_{P_p}/C_{\hat{c}}\| = \left\| \begin{pmatrix} (I - C_{\hat{c}}P_p)^{-1} & -(I - C_{\hat{c}}P_p)^{-1}C_{\hat{c}} \\ P_p(I - C_{\hat{c}}P_p)^{-1} & -P_p(I - C_{\hat{c}}P_p)^{-1}C_{\hat{c}} \end{pmatrix} \right\| \quad (13)$$

$$\leq \|P_p, I\| \left(\frac{\|(I, P_p)^T\| \|Q_{\hat{c}}L_{\hat{c}}\|}{1 - \sigma} + 1 \right). \quad (14)$$

The internal signals are bounded from their ideal values as

$$\|II_{P_{p^*}}/C_{\hat{c}}\| \leq \|II_{P_p}/C_{\hat{c}}\| \frac{1 + \delta(p, p^*)}{1 - \|II_{P_p}/C_{\hat{c}}\| \delta(p, p^*)}. \quad (15)$$

Proof. This is an extension of the 1-norm and ∞ -norm cases shown in Bradley (2010), to the 2-norm case. First set $w = (u_0, y_0 + y_{ref})^T$ in (10) and apply (4), (7) to give

$$\begin{aligned} [II_{P_p}/C_{\hat{c}}w](k) &= \begin{pmatrix} I \\ P_p \end{pmatrix} \left(\sum_{i=1}^k \left\{ [Q_{\hat{c}}(I - L_{\hat{c}}P_p)]^{i-1} (Q_{\hat{c}}L_{\hat{c}}y_{ref} \right. \right. \\ &\quad \left. \left. - Q_{\hat{c}}L_{\hat{c}}(P_p, -I)w_0(k-i)) \right\} + u_0(k) \right) \end{aligned}$$

and it follows that an upper bound on $\|II_{P_p}/C_{\hat{c}}\|$ is

$$\begin{aligned} &\left(\sum_{k=0}^{\infty} \left\| \begin{pmatrix} I \\ P_p \end{pmatrix} \sum_{i=1}^k [Q_{\hat{c}}(I - L_{\hat{c}}P_p)]^{i-1} Q_{\hat{c}}L_{\hat{c}}(-P_p, I) \right. \right. \\ &\quad \left. \left. \times w_0(k-i) + u_0(k) \right\|^2 \right)^{\frac{1}{2}} \\ &\sup_{\substack{w_0(k) \in \mathbb{R}^{m \times N \times n} \\ \|w_0\| \neq 0}} \left(\sum_{k=0}^{\infty} \|w_0(k)\|^2 \right)^{\frac{1}{2}} \end{aligned}$$

Setting $u_0 = 0$ and $y_0 = 0$ separately and applying relationship

$$\begin{aligned} \frac{\|II_{P_p}/C_{\hat{c}}w_0\|}{\|w_0\|} &= \frac{\|II_{P_p}/C_{\hat{c}}\begin{pmatrix} u_0 \\ 0 \end{pmatrix}\| + \|II_{P_p}/C_{\hat{c}}\begin{pmatrix} 0 \\ y_0 \end{pmatrix}\|}{\left\| \begin{pmatrix} u_0 \\ y_0 \end{pmatrix} \right\|} \\ &\leq \|II_{P_p}/C_{\hat{c}}|_{y_0=0}\| + \|II_{P_p}/C_{\hat{c}}|_{u_0=0}\| \end{aligned}$$

yields (14) after significant further manipulation. \square

Theorem 1 provides a transparent condition for robust stability of ILC. To illustrate this, suppose P_p is a plant model and \mathcal{U} is the uncertainty space specified by the designer as the set of all plants that must contain the unknown true plant P_{p^*} . Then (12) defines a gap ‘ball’ of plants that are stabilised by the ILC update (7). This is illustrated in Fig. 2. Relation (14) makes computation of the ball radius both simple and transparent: the designer must reduce σ as well as $\|Q_{\hat{c}}L_{\hat{c}}\|$ in order to reduce $\|II_{P_p}/C_{\hat{c}}\|$ and therefore increase the gap ball radius. Since reducing σ implies using a more aggressive ILC operator with larger gain, the role of the filter $Q_{\hat{c}}$ is key to increasing both robustness and convergence speed.

Remark 1. From (10), (15) it is evident that reducing $\|II_{P_p}/C_{\hat{c}}\|$ also reduces the sensitivity of the plant signals $(u_1, y_1)^T$ to external disturbances.

3. EMMILC framework

In practice, model-based ILC usually achieves better performance but has poor robustness against a general class of uncertainties, with a small gap radius $\|II_{P_p}/C_{\hat{c}}\|^{-1}$ generated by ILC update (7). EMMILC addresses this by introducing a set of ‘candidate’ plant models $\mathcal{P} = \{p_1, p_2, \dots, p_{N_p}\}$, where each is used to design an ILC controller $\hat{c} = K(p), \forall p \in \mathcal{P}$ with K denoting the ILC design procedure. The set of all ILC controllers is denoted $C = \{\hat{c}_1, \hat{c}_2, \hat{c}_3, \dots, \hat{c}_{N_p}\}$. Note that here state-space parameterisations p_i and \hat{c}_i refer to the systems P_{p_i} and $C_{\hat{c}_i}$ respectively.

By suitably switching between controllers, the aim is for EMMILC to guarantee bounded-input bounded-output stability for any true plant $P_{p^*} \in \mathcal{U}$. To decide on which ILC update to apply for each trial, a bank of Kalman estimators are designed to establish how well each plant model fits the measured data (u_2, y_2) . Each estimator $E(\hat{p})$ computes a residual, $r_{\hat{p}}$, equal to the size of the minimum disturbance necessary to explain the measurement (u_2, y_2) assuming that $P_{\hat{p}}$ is the true plant. Specifically, suppose $\mathcal{N}_{\hat{p}}^{[0,k]}(u_2, y_2)$ is the set of all disturbances (u_0, y_0) compatible with plant $P_{\hat{p}}$, the measured signals (u_2, y_2) and the signal connections in Fig. 1 over ILC trials $[0, k]$. The residual on trial k is then defined as

$$r_{\hat{p}}[k] = \inf \{r \geq 0 \mid r = \|v_0\|, v_0 \in \mathcal{N}_{\hat{p}}^{[0,k]}(u_2, y_2)\}. \quad (16)$$

Since ILC trials are independent, this can be calculated recursively as

$$r_{\hat{p}}[k] = \sqrt{(r_{\hat{p}}[k-1])^2 + (r_{\hat{p}}^k[N-1])^2}, \quad r_{\hat{p}}[0] = 0 \quad (17)$$

where the unlifted residual over interval $[0, t]$ on trial k is

$$r_{\hat{p}}^k[t] = \inf \{r \geq 0 \mid r = \|v_0\|, v_0 \in \mathcal{N}_{\hat{p}}^{[0,t]}(\tilde{u}_2(k, \cdot), \tilde{y}_2(k, \cdot))\}. \quad (18)$$

Here $\mathcal{N}_{\hat{p}}^{[0,t]}(\tilde{u}_2(k, \cdot), \tilde{y}_2(k, \cdot))$ is the unlifted equivalent of $\mathcal{N}_{\hat{p}}^{[0,k]}(u_2, y_2)$ on trial k . It is shown in Willems (2004) that (18) can be computed by the standard discrete-time unlifted Kalman filter using the unlifted ‘along-the-trial’ update

$$\begin{aligned} \tilde{x}_p(t+1/2) &= \tilde{x}_p(t) - \Sigma_p(t)C_p^T [C_p \Sigma_p(t)C_p^T + I]^{-1} \\ &\quad \cdot [\tilde{y}_2(k, t) + C_p \tilde{x}_p(t)] \end{aligned} \quad (19)$$

$$\begin{aligned} \Sigma_p(t+1/2) &= \Sigma_p(t) - \Sigma_p(t)C_p^T [C_p \Sigma_p(t)C_p^T + I]^{-1} \\ &\quad \cdot C_p \Sigma_p(t) \end{aligned} \quad (20)$$

$$\tilde{x}_p(t+1) = A_p \tilde{x}_p(t+1/2) + B_p(\tilde{u}_2(k, t)) \quad (21)$$

$$\Sigma_p(t+1) = A_p \Sigma_p(t+1/2)A_p^T + B_p B_p^T \quad (22)$$

with initial conditions $\Sigma_p(0)$, $\tilde{x}_p(0)$ and sample $t \in [0, N-1]$. The required $r_{\hat{p}}^k[N-1]$ is then given by the weighted norm

$$r_{\hat{p}}^k[N-1] = \left[\sum_{t=0}^{N-1} \|\tilde{y}_2(k, t) + C_p \tilde{x}_p(t)\|_{[C_p \Sigma_p(t)C_p^T + I]^{-1}}^2 \right]^{\frac{1}{2}}. \quad (23)$$

Computations (17), (19)–(23) incur far less load than solving (16) since they do not involve large matrices.

The ILC update corresponding to the candidate plant with the smallest residual is then used to compute the next trial’s control input. The switching signals is therefore defined by

$$q(k) := \arg \min_{p \in \mathcal{P}} r_{\hat{p}}[k] \quad \forall k \in \mathbb{N} \quad (24)$$

with corresponding ILC operator $C_{K(q(k))}$. The overall EMMILC scheme is illustrated by Fig. 3.

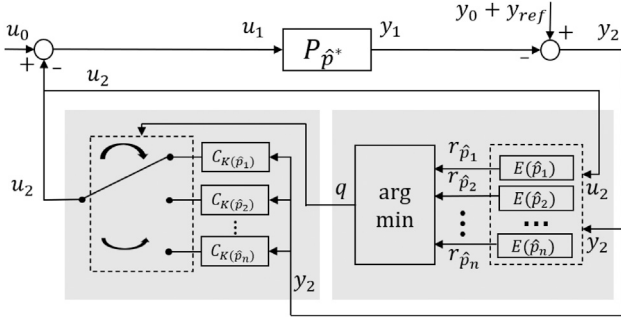


Fig. 3. EMMILC framework: the bank of estimators $E(\cdot)$ defined by (17), (19)–(23) outputs the residuals $r_{\hat{p}_1}$ to $r_{\hat{p}_n}$, the minimum residual is used to produce the switching signal q , which then selects the next ILC update to apply to P_p .

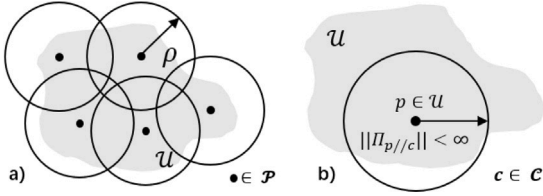


Fig. 4. (a) Uncertainty set \mathcal{U} covered by balls of radius ρ . (b) Every plant $p \in \mathcal{U}$ has a stabilising controller $\hat{c} \in \mathcal{C}$.

3.1. EMMILC robust performance conditions

Conditions for the stability of EMMILC were derived in Freeman and French (2015), including bounds on the internal signals. However they involved a substantial computational load that made them infeasible to use in practice. Here they are presented in a simpler form suitable for subsequently developing an efficient design framework.

Theorem 2. Let true plant $P_{p^*} \in \mathcal{U}$. Let \mathcal{P} be a set of candidate plant models of form (1) and \mathcal{C} a set of corresponding ILC controllers designed using (7) such that (8) holds. Then the EMMILC implementation defined by (17), (19)–(24) stabilises the true plant provided the following two conditions are met:

1. The candidate model set \mathcal{P} satisfies

$$\exists p \in \mathcal{P}, \quad \text{s.t.} \quad \delta(p, p^*) < \rho(\mathcal{P}, \mathcal{C}, \mathcal{U}), \quad (25)$$

where ρ is a positive scalar function of the controller set \mathcal{C} , plant set \mathcal{P} and uncertainty space \mathcal{U} .

2. The set of controllers \mathcal{C} satisfies

$$\exists \hat{c} \in \mathcal{C}, \quad \text{s.t.} \quad \|\Pi_{\hat{p}/\hat{c}}\| < \infty \quad \forall p \in \mathcal{U}. \quad (26)$$

In particular, the controller signals of the switched closed-loop system $[P_{\hat{p}^*}, C_{K(q)}]$ are bounded with respect to their ideal values as

$$\|w_2\|_{(-P_{\hat{p}^*}^{-1}, 0)^T} < \eta(\mathcal{P}, \mathcal{C}, \mathcal{U}) \|w_0\|, \quad (27)$$

where η is a positive scalar function defined in Freeman and French (2015).

Proof. This is a simplified restatement of Freeman and French (2015) which contains the full computation of functions ρ and η . Note that EMMILC is an extension of the MMAC framework developed in Buchstaller and French (2016a) for feedback stabilisation. \square

The two conditions (25), (26) guarantee robust performance of EMMILC when applied to an unknown plant $P_{p^*} \in \mathcal{U}$, and can be interpreted as follows:

Condition (1) specifies a minimum radius of gap balls covering the uncertainty space, and hence dictates the number of estimators required. It is illustrated by Fig. 4(a).

Condition (2) states that there must exist a stabilising controller for each plant in set \mathcal{U} . This is illustrated in Fig. 4(b).

3.2. EMMILC design procedure

Computing $\rho(\mathcal{P}, \mathcal{C}, \mathcal{U})$ entails a large computational burden, and is also conservative (i.e. more candidate plants are specified than required). To address this, an efficient design procedure is now developed, which does not explicitly require calculating $\rho(\mathcal{P}, \mathcal{C}, \mathcal{U})$.

Firstly, criterion (26) requires every plant in the uncertainty set \mathcal{U} to be stabilised by at least one of the controllers in \mathcal{C} . The obvious approach to satisfy this is using the stability bound (12) to design a minimal candidate plant set \mathcal{P} whose gap balls (each with radius $\|\Pi_{\hat{p}/K(p)}\|^{-1}$) cover the uncertainty space \mathcal{U} . This is achieved by using Theorem 1, i.e. selecting a radius for each ball of

$$\rho = \gamma \|\Pi_{\hat{p}/\hat{c}}\|^{-1}, \quad (28)$$

where $\gamma = 1$. This can be used to design a candidate plant set which satisfies criterion (26), however, criterion (25) may not be satisfied. Hence the tuning parameter $0 < \gamma \leq 1$ will be employed to reduce the radius of the gap balls. As $\gamma \rightarrow 0$, more gap balls will be included to cover the same set \mathcal{U} , hence (25) will always be satisfied for any possible ρ , avoiding the need to calculate it.

To compute the minimal set of candidate plants that cover set \mathcal{U} , a practical approach is to first define the largest set of plant models that resources permit, denoted $\mathcal{H} = \{p_1, p_2, \dots, p_{N_m}\}$. These are uniformly distributed in the uncertainty space \mathcal{U} . Then, $\gamma = 1$ is chosen to satisfy criterion (26). For each $p \in \mathcal{H}$, (28) is computed and other plants are removed which are within this radius of p , as measured by the gap metric. If criterion (25) is not satisfied, the value of γ is reduced and this process is repeated. When all unnecessary models are removed, the minimal set \mathcal{P} is obtained. The overall approach is stated in Algorithm 1, where the ILC controller set \mathcal{C} is produced using the resulting minimal plant set. The principle is illustrated by Fig. 5.

Algorithm 1 Design Procedure.

Require: ILC design procedure K , uncertainty space \mathcal{U} and tunable parameter $0 < \gamma \leq 1$

Ensure: Minimal candidate plant set \mathcal{P}

- 1: Define $\mathcal{H} = \{p_1, \dots, p_{N_m}\}$ as the finest grid to cover \mathcal{U} ;
- 2: Set $S = \{0, 0, \dots, 0\}$ with N_m elements, S_j denoting the j^{th} element;
- 3: **for each** $i \in \{1, 2, 3, \dots, N_m\}$ **do**
- 4: **for each** $j \in \{1, 2, 3, \dots, N_m\}$ **do**
- 5: **if** $\exists a \in \{1, 2, 3, \dots, N_m\}$, s.t. $S_a = 0$ **then**
- 6: Design $Q_{\hat{c}_i}, L_{\hat{c}_i}$ for $\hat{c}_i = K(p_i)$ to reach a compromise between minimising (14) and (8).
- 7: **if** $\delta(\hat{p}_i, \hat{p}_j) < \gamma \|\Pi_{\hat{p}_i/K(p_i)}\|^{-1}$ **then**
- 8: $S_j = i$;
- 9: **end if**
- 10: **else**
- 11: Delete repetitions from S , set $N_p = |S|$;
- 12: $\mathcal{P} = \{P_{p_{S_1}}, P_{p_{S_2}}, \dots, P_{p_{S_{N_p}}}\}$; Exit loops;
- 13: **end if**
- 14: **end for**
- 15: **end for**
- 16: Return \mathcal{P} .

4. Model description

This section defines the structure of the wrist dynamics, together with a suitable procedure to identify the uncertainty space \mathcal{U} required by the EMMILC design procedure.

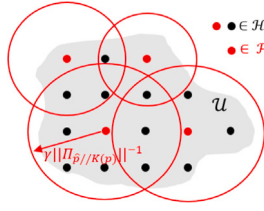


Fig. 5. The black and red plant models comprise the initial candidate plant model set \mathcal{H} and are spread uniformly across uncertainty set \mathcal{U} . The black plant models are not needed and are removed from the set \mathcal{H} . The remaining red plants form the minimal candidate plant model set \mathcal{P} , which still covers \mathcal{U} . (For interpretation of the references to colour in this figure legend, the reader is referred to the web version of this article.)

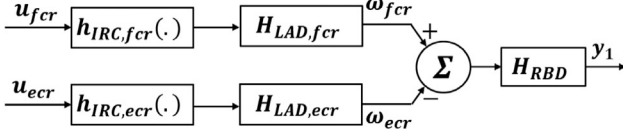


Fig. 6. Wrist model excited by stimulation inputs u_{fcr} and u_{ecr} to wrist flexor and extensor muscles respectively, with output torques ω_{fcr} and ω_{ecr} . Output y_1 is the wrist angle.

4.1. Stimulated wrist dynamics

The rehabilitation aim is to enable the wrist angle to follow a desired trajectory using electrical stimulation applied to muscles in the forearm. Bi-directional wrist movement is achieved via stimulation of the Flexor Carpi Radialis (FCR) and Extensor Carpi Radialis (ECR) muscles. The torque produced by each muscle can be modelled as a Hammerstein structure, comprising a static non-linearity which comprises the isometric recruitment curve (IRC), in series with linear activation dynamics (LAD). The IRC can be modelled as piecewise linear function, with segments corresponding to the deadzone, contraction, and saturation characteristics of the muscle (Le, Markovskiy, Freeman, & Rogers, 2010). The fixed transition between deadzone and linear region can be readily measured and will be denoted $u_{c,fcr}$, $u_{c,ecr}$ for ECR and FCR, respectively. The gradient of the contraction region will be likewise denoted α and β . The LAD component is typically modelled as a critically damped second order system (Gföhler, Angeli, & Lugner, 2004; Rouhani, Popovic, Same, Li, & Masani, 2016), and will be denoted $H_{LAD,fcr}(s)$ and $H_{LAD,ecr}(s)$ for the FCR and ECR respectively. The resulting torque is summed and feeds into the rigid body dynamics (RBD) of the wrist, denoted H_{RBD} . These can be parameterised by damping, B_s , stiffness, K_s , and inertia I_s values (Copur, Freeman, Chu, et al., 2016). The overall model structure is shown in Fig. 6.

To produce a single input system, a static function is added to split the control signal $u_1(t)$ between the two muscles. This strategy is known as co-activation, and is widely used in FES-based upper-limb studies (Bó, da Fonseca, & de Sousa, 2016; Copur et al., 2016; Klauer, Ambrosini, Ferrante, et al., 2019). It replicates natural human motor control, and therefore reinforces the rehabilitation aim. However, to avoid fatigue it is necessary to minimise the level of co-activation of antagonistic muscles while effectively compensating for the dead-zone (Schauer, 2017). In general, the co-activation level should be minimised to avoid impeding movement and hastening fatigue (Zhang, Chu, Liu, et al., 2020). In addition, it reduces the operational range of $u_1(t)$ and the angular response. The co-activation function hence takes the form

$$u_{fcr}(t) = \begin{cases} u_1(t) + u_{c,fcr}, & 0 \leq u_1(t) \leq 300 - u_{c,fcr} \\ u_{c,fcr}, & u_{c,ecr} - 300 \leq u_1(t) < 0 \end{cases} \quad (29)$$

$$u_{ecr}(t) = \begin{cases} u_{c,ecr}, & 0 \leq u_1(t) \leq 300 - u_{c,fcr} \\ u_{c,ecr} - u_1(t), & u_{c,ecr} - 300 \leq u_1(t) < 0 \end{cases} \quad (30)$$

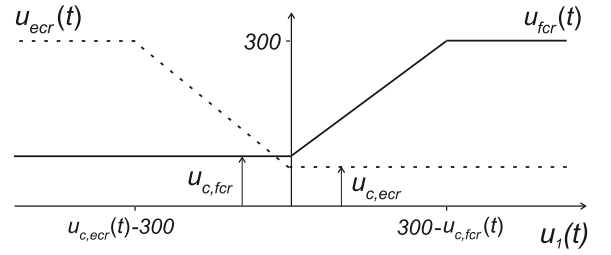


Fig. 7. Co-activation function with levels $u_{c,fcr}$, $u_{c,ecr}$.

where co-activation levels $u_{c,fcr}$, $u_{c,ecr} \geq 0$ are the twitch responses measured during calibration (i.e. the stimulation values just before torque is produced). The co-activation function is illustrated by Fig. 7. For simplicity it is assumed the stimulation amplitude is set such that saturation occurs above the maximal stimulation pulsewidth (300 μ s).

With the co-activation function applied, the overall system model can then be written as the operator $P_p : u_1 \mapsto y_1$, where

$$w = h_{IRC}(u_1) := \begin{cases} \alpha u_1, & u_1 \geq 0 \\ \beta u_1, & u_1 < 0 \end{cases}, \quad (31)$$

$$Y_1(s) = \underbrace{\frac{1}{I_s s^2 + B_s s + K_s}}_{RBD} \underbrace{\frac{\omega_n^2}{s^2 + 2\omega_n s + \omega_n^2}}_{H_{LAD}} W(s), \quad (32)$$

where $X(s)$ denotes the Laplace transformed signal $x(t)$ in the time domain. This linear model form simplifies the identification and candidate model design procedures described in the next section, but it reduces accuracy due to neglecting non-linearities in the damping and friction terms. However, due to the relatively slow dynamics of human movement, their effect is not significant in the current scenario (Freeman, Hughes et al., 2009).

4.2. System identification

This section defines a suitable procedure to identify the parameters in the wrist model (32), (31).

Definition 1 (Identification Problem). Suppose an FES sequence $\{\tilde{u}_1(t)\}_{t=1}^N$ is applied to system (32), (31) generating the measured output signal $\{\tilde{y}_1(t)\}_{t=1}^N$. The overall input/output data set with length N is defined as

$$Z^N = \{\tilde{u}_1(1), \tilde{y}_1(1), \tilde{u}_1(2), \tilde{y}_1(2), \dots, \tilde{u}_1(N), \tilde{y}_1(N)\}. \quad (33)$$

Then the parameters are the solution to the cost optimisation problem

$$p := \min_{(K_s, I_s, B_s, \omega_n, \alpha, \beta)} \sum_{t=1}^N (\tilde{y}_1(t) - \tilde{y}'_1(t))^2, \quad (34)$$

where $(\tilde{u}_1, \tilde{y}_1) \in Z^N$, and \tilde{y}'_1 is computed using

$$\begin{aligned} x(t+1) &= A_d x(t) + B_d h_{IRC}(\tilde{u}_1(t)) \\ \tilde{y}'_1(t) &= C_d x(t), \quad t = 0, 1, 2 \dots \end{aligned} \quad (35)$$

where

$$A_d = e^{A_c T_s}, \quad B_d = (e^{A_c T_s} - I) A_c^{-1} B_c, \quad C_d = C_c, \quad (36)$$

is the discrete representation of system (32), which has state-space realisation (A_c, B_c, C_c) where

$$\begin{aligned} A_c &= \begin{bmatrix} 0 & 1 & 0 & 0 \\ 0 & 0 & 1 & 0 \\ 0 & 0 & 0 & 1 \\ -a_0 & -a_1 & -a_2 & -a_3 \end{bmatrix}, \quad B_c = \begin{bmatrix} 0 \\ 0 \\ 0 \\ 1 \end{bmatrix}, \\ C_c &= [b_0 \quad 0 \quad 0 \quad 0], \end{aligned} \quad (37)$$

Table 1
Quantified performance PI_{50} and PI_{10} values for each subject with AE and ME electrode positions.

Subject	Standard ILC				EMMILC			
	AE(PI_{50})	AE(PI_{10})	ME(PI_{50})	ME(PI_{10})	AE(PI_{50})	AE(PI_{10})	ME(PI_{50})	ME(PI_{10})
a	14.94	4.75	23.17	7.67	13.95	5.81	15.11	5.77
b	16.33	5.98	23.44	7.55	12.32	3.68	12.09	4.06
c	16.42	4.93	21.94	5.45	16.39	4.91	14.88	4.67
d	30.94	7.69	105.11 (diverging)	9.35	26.76	7.96	32.54	8.89

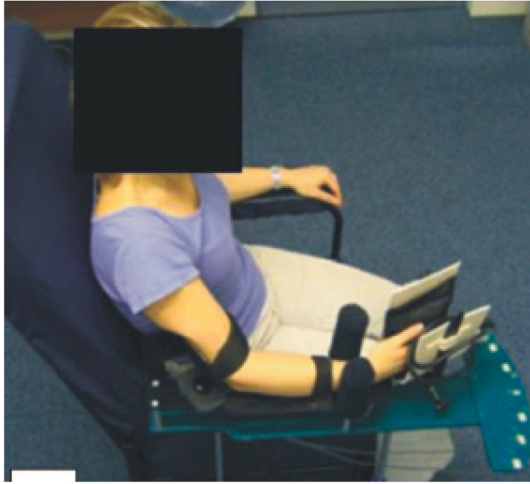


Fig. 8. Experimental set-up showing test subject seated in the validated wrist rig (permission received from Turk et al., 2008).

with $b_0 = \omega_n^2/I_s$, $a_0 = (\omega_n^2 K_s)/I_s$, $a_1 = (2\omega_n K_s + \omega_n^2 B_s)/I_s$, $a_2 = (K_s + 2\omega_n B_s + \omega_n^2 I_s)/I_s$, $a_3 = (B_s + 2I_s \omega_n)/I_s$.

4.3. Model uncertainty set

This section defines a suitable procedure to construct a candidate plant set by solving the **Identification Problem**.

Definition 2 (Uncertainty Set Computation). Suppose a collection of m sufficiently varied identification data sets Z_i^N has been collected, each of form (33). For each set $i = 1, 2, \dots, m$, solve the **Identification Problem** to generate $(K_{s,i}, I_{s,i}, B_{s,i}, \omega_{n,i}, \alpha_i, \beta_i)$. Then a convex set containing all individual models p_i can be computed as

$$\mathcal{U} := \{ P_p | p = (K_s, I_s, B_s, \omega_n, \alpha, \beta), K_s \in \mathcal{K}, I_s \in \mathcal{I}, B_s \in \mathcal{C}, \omega_n \in \mathcal{W}, \alpha \in \mathcal{A}, \beta \in \mathcal{B} \}, \quad (38)$$

where the individual parameter variation sets are $\mathcal{K} := [\min_i \{K_{s,i}\}, \max_i \{K_{s,i}\}]$, $\mathcal{I} := [\min_i \{I_{s,i}\}, \max_i \{I_{s,i}\}]$, $\mathcal{C} := [\min_i \{B_{s,i}\}, \max_i \{B_{s,i}\}]$, $\mathcal{W} := [\min_i \{\omega_{n,i}\}, \max_i \{\omega_{n,i}\}]$, $\mathcal{A} := [\min_i \{\alpha_i\}, \max_i \{\alpha_i\}]$, $\mathcal{B} := [\min_i \{\beta_i\}, \max_i \{\beta_i\}]$. The set \mathcal{U} is then fed into Algorithm 1 to construct the desired candidate plant model set.

5. Experimental test procedure

EMMILC is now applied to the common rehabilitation scenario in which FES supports wrist flexion and extension during a reach, grasp and return motion. The test subject places their arm in the instrumented wrist rig described in Turk, Notley, Pickering, Simpson, Wright, and Burrige (2008) and shown in Fig. 8. This supports their arm and restricts movement to only the horizontal plane. The reference y_{ref} is a smooth 20° wrist motion of duration 8 seconds. The subject's wrist is manually reset to 0° between trials, in order to guarantee identical initial conditions.

FES surface electrodes (Pals PLUS, 5×5 cm) are first applied to FCR and ECR muscles using the aligned electrode (AE) positions shown in

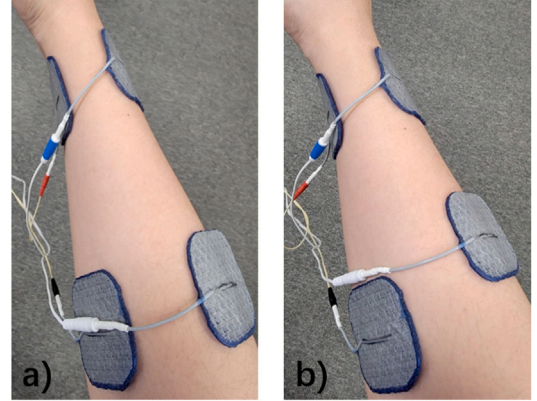


Fig. 9. Electrode placements: (a) AE and (b) ME positions.

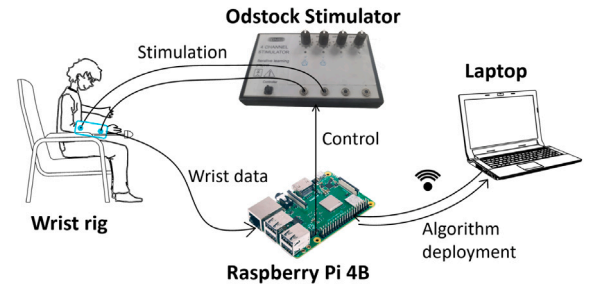


Fig. 10. Upper-limb FES system components.

Fig. 9 (a). Then Standard ILC and EMMILC will be applied and their performance compared. To replicate real conditions over a programme of rehabilitation, a sufficiently large number of ILC trials will be run to elicit significant fatigue. After a period of rest, both tests will be repeated using the misaligned electrode (ME) positions shown in Fig. 9 (b) in order to replicate the variation in electrode placement that would naturally occur in clinical practice.

The hardware and suitable experimental procedure to compute the uncertainty set (using the results of Section 4) and subsequent EMMILC implementation (using the design framework of Section 3) are now described.

5.1. Experimental system

The wrist angle is measured using a resolver, with range $[-90^\circ, 90^\circ]$ and transmitted to a Raspberry Pi 4B board (Raspberry Pi Foundation, UK). This runs the software which is programmed using the Matlab/SIMULINK toolbox for Raspberry Pi. This low-cost portable hardware is chosen since the system will ultimately be deployed in the homes of stroke patients. The control software generates two 40 Hz pulse-width modulated (PWM) square wave signals, whose pulsewidth corresponds to signals u_{fcr} and u_{ecr} in Fig. 6. These signals have a maximum value of $300 \mu s$ and are amplified by a commercial stimulator (Odstock Medical Limited, UK) which outputs the resulting high voltage pulse-train to the electrode pairs. The sampling frequency in all tests is 40 Hz. The system components are shown in Fig. 10.

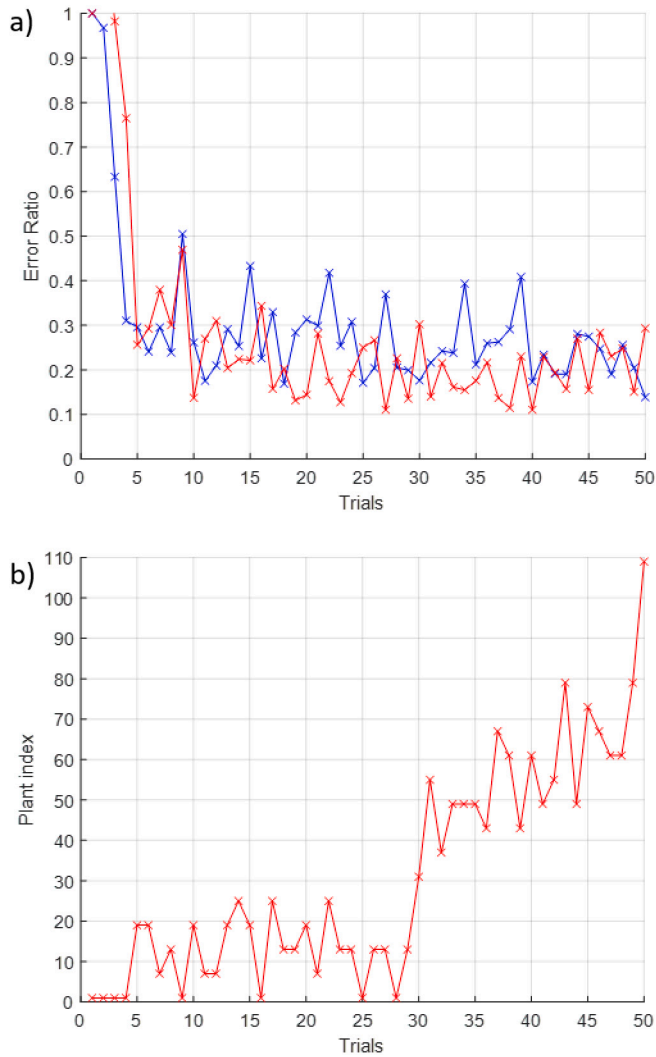


Fig. 11. (a) [Red line] Tracking error ratio of EMMILC in each trial with standard electrode positioning. [Blue line] Tracking error ratio of Standard ILC in each trial with standard electrode positioning. (b) Switched plant for EMMILC in each trial. (For interpretation of the references to colour in this figure legend, the reader is referred to the web version of this article.)

5.2. Design of the candidate plant set

To design a candidate plant set, the first step will be to define the uncertainty space. The **Uncertainty Set Computation** will be run with the input component $\tilde{u}_{1,i}$ of each set Z_i^N taking the form of a sequence of sine-wave signals with frequencies comprising 0.7 Hz, 1.1 Hz, 1.5 Hz, 1.9 Hz, and 2.3 Hz. These frequencies are chosen to sufficiently excite the wrist while also ensuring comfort. Physiological variation will be captured by performing the identification test seven times (over 15 minutes) per day using a different electrode placement each time. This guarantees the model identified can capture highly fatigued conditions (Brend, 2014). This will be repeated over seven days to capture the full day-to-day variation in patient physiology. The resulting collection of $m = 49$ data sets, Z_i^N , and respective models, p_i , will be used to compute \mathcal{U} via (38).

For each identification, fitting accuracy will be defined as

$$F_{p_i} = \left(1 - \frac{\|\tilde{y}_{1,i} - \tilde{y}'_{1,i}\|}{\|\tilde{y}_{1,i}\|} \right) \times 100, \quad (39)$$

where $\tilde{y}'_{1,i}$ is the result of applying $\tilde{u}_{1,i}$ to model p_i . Each input $\tilde{u}_{1,i}$ will be applied twice and only the first data set will be used for identification.

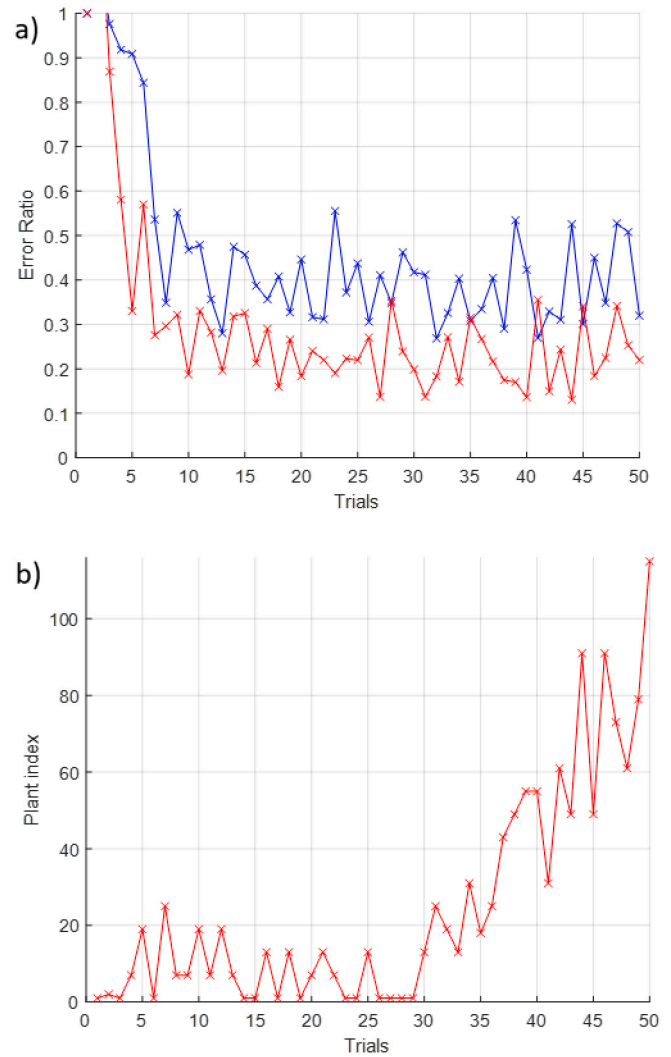


Fig. 12. (a) [Red line] Tracking error ratio of EMMILC in each trial with misaligned electrode positioning. [Blue line] Tracking error ratio of Standard ILC in each trial with misaligned electrode positioning. (b) Switched plant for EMMILC in each trial. (For interpretation of the references to colour in this figure legend, the reader is referred to the web version of this article.)

The second will be used purely to compute a prediction accuracy which will be termed V_{p_i} .

Having identified uncertainty set \mathcal{U} , the next step is to define the control design procedure used in Algorithm 1. Here the norm optimal ILC algorithm is chosen, due to its success in five clinical trials using FES for upper limb rehabilitation (Freeman, 2016).

For a plant model p , this corresponds to the ILC update C_ϵ , where $\hat{c} = K(p)$ is given by

$$u_2(k+1) = Q_\epsilon(u_2(k) - (I + \beta P_\rho P_\rho^T)^{-1} \beta P_\rho^T y_2(k)), \quad (40)$$

which has a convergence condition satisfying (8). The filter Q_ϵ is designed as a 5th order zero-phase low-pass filter with cut-off frequency 3 Hz in order to remove frequencies that are not contained in the reference. This hence maximises robustness bound (14). The step size $\beta = 0.001$ is chosen as a suitable compromise between robustness (14) and convergence (8) as required by Algorithm 1.

Within Algorithm 1, the parameter $\gamma = 1$ is chosen to investigate the coarsest candidate model set. Also, $N_m = 120$ is specified as the initial plant set size \mathcal{H} since it is the maximum the hardware can support.

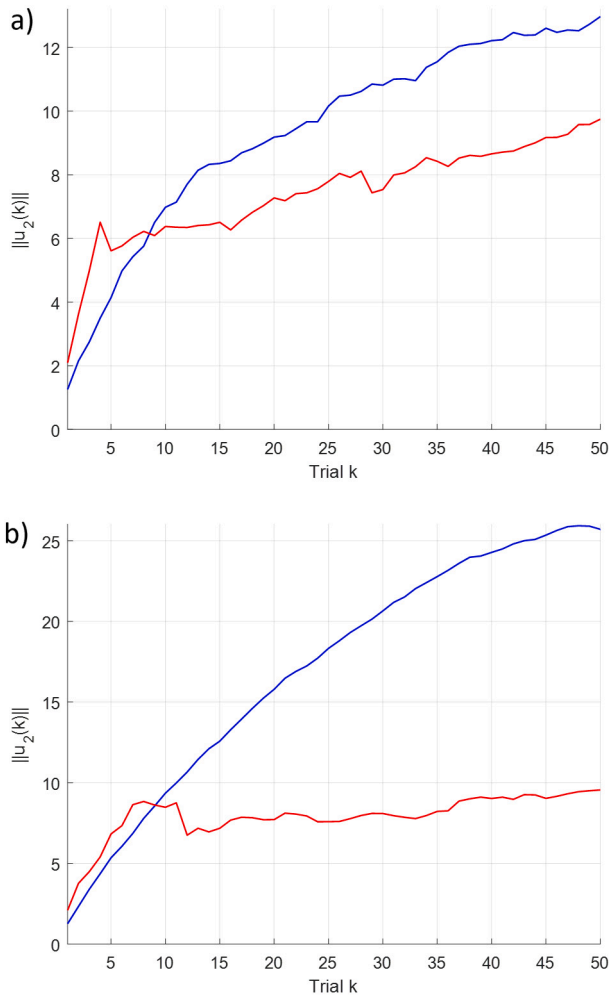


Fig. 13. (a) [Red line] Control energy $\|u_2(k)\|$ of EMMILC in trial k with AE positioning. [Blue line] Control energy $\|u_2(k)\|$ of standard ILC in trial k with AE positioning. (b) As above but with ME positioning. (For interpretation of the references to colour in this figure legend, the reader is referred to the web version of this article.)

When applied to track y_{ref} , the control performance will be quantified by a performance index

$$PI_{N_k} = \sum_{k=1}^{N_k} \frac{\|y_2(k)\|}{\|y_{ref}\|}, \quad (41)$$

where N_k denotes a total trial number of interest. This index accumulates the error ratio over the first N_k trials and captures both convergence speed and final tracking accuracy (Ratcliffe, Lewin, Rogers, Hatonen, & Owens, 2006). The smaller the value of PI_{N_k} , the better the tracking performance over the N_k trials.

6. Experimental results

Ethics approval was granted by University of Southampton Ethics and Research Governance Online (ERGO), ID 72855. Four unimpaired subjects were recruited, as a prerequisite for later clinical tests with stroke patients. The subjects were seated and electrodes were placed in the AE position as previously described. A stimulation pulsewidth of 300 μ s was applied to each muscle in turn, and the amplitude was slowly increased to a maximum comfortable limit. The pulsewidth was then set to zero, and is the controlled variable. The stimulation levels corresponding to the twitch response of each muscle were then measured to determine the co-activation levels $u_{c,fer}$, $u_{c,cer}$. The experimental results are now given.

6.1. Identification results

The procedure described in Section 5.2 was applied to construct the candidate model set. It was decided to perform this with only one subject, in order to evaluate whether a single candidate model set could yield satisfactory performance with all subjects. If successful, this would effectively remove the need for model identification and hence constitute a major step towards achieving model-free, home-based FES rehabilitation.

Having collected data sets Z_i^N , the corresponding $m = 49$ identified models had a fitting accuracy range of 61% – 71% and a validation accuracy range of 59% – 68%, computed using (39). Applying the **Uncertainty Set Computation** yielded the overall uncertainty set

$$\mathcal{U} := \{P_p | p = (K_s, I_s, B_s, \omega_n, \alpha, \beta), K_s \in [0.01, 0.08], I_s \in [0.00001, 0.0001], B_s \in [0.001, 0.01], \omega_n \in [5, 15], \alpha \in [0.6, 1.2], \beta \in [0.9, 1.1]\}. \quad (42)$$

Taking the controller form (40) within Algorithm 1 then produced a minimal candidate set $\mathcal{P} = \{p_1, p_2, \dots, p_{N_p}\}$ comprising $N_p = 116$ plants (4 having been removed).

6.2. Performance with AE placement

The first tests compare standard ILC with EMMILC for all subjects using AE positioning. Standard ILC requires a new model to be identified. Therefore the **Identification Problem** was solved for each subject by applying stimulation input \bar{u}_1 designed in Section 5.2. The resulting identified model was then lifted to give $P_{\hat{p}}$ which was applied with standard ILC update (40) to track y_{ref} over 50 trials.

After a 20-minute rest, EMMILC was then performed over 50 trials using the same candidate set defined above for each subject. The tracking performance for each subject is shown in Table 1.

This shows that all subjects performed better using EMMILC, as the PI_{50} values are smaller than those of standard ILC. Specifically, Fig. 11 shows the results with subject *a*, where EMMILC has approximately 25% better performance. In terms of the convergence over the initial 10 trials, measured using PI_{10} , EMMILC provides similar performance compared with standard ILC.

Fig. 13 (a) shows the control effort $\|u_2(k)\|$ applied to subject *b* over trial $k = 1, 2, \dots, 50$ using standard ILC and EMMILC. In both cases the FES energy increases over time due to muscle fatigue. However, this continuous increase of stimulation increases patient discomfort, especially in the case of standard ILC. In comparison, EMMILC has reduced the stimulation required by using the most accurate plant model on every trial, thereby minimising energy. In contrast, standard ILC has employed an inaccurate plant model which wastes effort by exciting modes/frequencies not required by the task.

In a home-use or wearable scenarios there is limited processing power, meaning that fewer candidate plant models can be supported. To investigate the effect of limited computational resources, EMMILC was next redesigned to have fewer candidate plants. This was achieved by designing $Q_{\hat{c}}$ in Algorithm 1 to reduce robustness when minimising (14) and hence cover the uncertainty space with fewer candidate plants. As a compromise, the convergence rate of each plant model is reduced. To examine this, four candidate sets were produced with a descending number of plants. Each of them was applied on one subject with AE positioning over 50 trials. The results are then presented in Table 2.

The results show that the tracking performance of EMMILC reduces as the number of candidate plants (and hence computational load) reduces. Comparison between Tables 2 and 1 shows that, even with only 30 models, the performance of EMMILC is still superior to that of standard ILC. This supports the efficacy of EMMILC to be used for home-based FES rehabilitation. However, the subject reported a larger oscillation of wrist movements as the number of candidate models decreased, slightly reducing comfort during testing.

Table 2
Quantified performance for four different plant sets.

Plant set	No. plants	PI_{50} value
P_1	$N_p = 116$	12.32
P_2	$N_p = 97$	13.81
P_3	$N_p = 71$	14.03
P_4	$N_p = 30$	14.66

6.3. Performance with ME placement

The test procedure was then repeated with the ME position. Results show that EMMILC significantly outperformed standard ILC, which could not stabilise the system with subject d . This is manifested in both short-term (PI_{10}) and long-term (PI_{50}) convergence in Table 1. These results are remarkable given that the candidate plant set used for all subjects was built only for subject b . This confirms the possibility that no further identification is required for different subjects.

To illustrate the switching process, the tracking results of subject a are shown for AE (Fig. 11) and ME (Fig. 12), positioning. As in Fig. 11 (a), standard ILC decreased its tracking error to 26% of its initial value within 10 trials. In comparison, EMMILC required 10 trials to reach 14% of its initial value. The switching process is shown Fig. 11 (b), where the change in wrist dynamics started to increase after trial 29. EMMILC adapted to this by switching to other candidate plants. As shown in Fig. 12 (a), EMMILC decreased to 19% of its initial error after 10 trials, but standard ILC decreased to only 47% of its initial error. Similarly, EMMILC also adapted to the increased physiological variation following trial 29, as shown in Fig. 12 (b).

Fig. 13 (b) shows the control effort used by each ILC type. EMMILC clearly applied much smaller stimulation inputs to subject b compared to standard ILC with ME positioning, illustrating that it can deal with fatigue much more effectively. EMMILC also achieved far better performance with ME positioning, as shown in Table 1.

7. Conclusion

This paper has addressed the key problem of FES-based upper-limb rehabilitation by implementing a multiple-model adaptive framework. Building on the initial numerical results in Zhou, Freeman, and Holderbaum (2023b) and Zhou et al. (2023a), it combined an efficient design procedure with EMMILC to transparently balance computational burden and tracking performance. By using this protocol, this research has designed a candidate plant model set which can be applied to all subjects. This removes time-consuming identification tests, and hence increases the possibility of accurate FES control when progressing to home-use scenarios. The EMMILC framework has been experimentally tested with four healthy test subjects and has automatically adapted to their fatigue and electrode re-positioning. As a result, EMMILC has improved performance by 28% compared to standard ILC. Future investigations will involve EMMILC with higher dimensional multiple-input, multiple-output systems (e.g. electrode arrays), which have greater muscle selectivity and can provide intensive and goal-oriented FES training that supports a variety of upper-limb activities.

CRediT authorship contribution statement

Junlin Zhou: Writing – review & editing, Writing – original draft, Visualization, Validation, Software, Resources, Project administration, Methodology, Investigation, Formal analysis, Data curation, Conceptualization. **Christopher T. Freeman:** Writing – review & editing, Supervision, Resources, Methodology, Conceptualization. **William Holderbaum:** Writing – review & editing, Supervision, Resources, Conceptualization.

Declaration of competing interest

The authors declare that they have no known competing financial interests or personal relationships that could have appeared to influence the work reported in this paper.

References

- Ahn, H., Moore, K. L., & Chen, Y. (2005). Schur stability radius bounds for robust iterative learning controller design. In *Proceedings of the 2005 American control conference: vol. 1*, (pp. 178–183).
- Alibeji, N., Kirsch, N., Dicianno, B. E., & Sharma, N. (2017). A modified dynamic surface controller for delayed neuromuscular electrical stimulation. *IEEE/ASME Transactions on Mechatronics*, 22(4), 1755–1764.
- Allen, B. C., Cousin, C. A., Rouse, C. A., & Dixon, W. E. (2022). Robust cadence tracking for switched FES-cycling with an unknown time-varying input delay. *IEEE Transactions on Control Systems Technology*, 30(2), 827–834.
- Allen, B. C., Stubbs, K. J., & Dixon, W. E. (2022). Data-based and opportunistic integral concurrent learning for adaptive trajectory tracking during switched FES-induced biceps curls. *IEEE Transactions on Neural Systems and Rehabilitation Engineering*, 30, 2557–2566.
- Anderson, K. D. (2004). Targeting recovery: Priorities of the spinal cord-injured population. *Journal of Neurotrauma*, 21(10), 1371–1383.
- Arimoto, S., Kawamura, S., & Miyazaki, F. (1984). Bettering operation of dynamic systems by learning: A new control theory for servomechanism or mechatronics systems. In *The 23rd IEEE conference on decision and control* (pp. 1064–1069).
- Ballester, B. R., Ward, N. S., Brander, F., et al. (2022). Relationship between intensity and recovery in post-stroke rehabilitation: A retrospective analysis. *Journal of Neurology, Neurosurgery and Psychiatry*, 93(2), 226–228.
- Bó, A. P. L., da Fonseca, L. O., & de Sousa, A. C. C. (2016). FES-induced co-activation of antagonist muscles for upper limb control and disturbance rejection. *Medical Engineering & Physics*, 38(11), 1176–1184.
- Bradley, R. S. (2010). *The robust stability of iterative learning control* (Ph.D. thesis), University of Southampton.
- Brend, O. (2014). *Implementation and experimental evaluation of multiple model switched adaptive control for FES-based rehabilitation* (Ph.D. thesis), University of Southampton.
- Brend, O., Freeman, C. T., & French, M. (2015). Multiple-model adaptive control of functional electrical stimulation. *IEEE Transactions on Control Systems Technology*, 23(5), 1901–1913.
- Bristow, D. A., Tharayil, M., & Alleyne, A. G. (2006). A survey of iterative learning control. *IEEE Control Systems Magazine*, 26(3), 96–114.
- Buchstaller, D., & French, M. (2016a). Robust stability for multiple model adaptive control: Part I—The framework. *IEEE Transactions on Automatic Control*, 61(3), 677–692.
- Buchstaller, D., & French, M. (2016b). Robust stability for multiple model adaptive control: Part II—Gain bounds. *IEEE Transactions on Automatic Control*, 61(3), 693–708.
- leung Chan, M. K., yu Tong, R. K., & kwan Chung, K. Y. (2009). Bilateral upper limb training with functional electric stimulation in patients with chronic stroke. *Neurorehabilitation and Neural Repair*, 23(4), 357–365.
- Copur, E. H., Freeman, C. T., Chu, B., et al. (2016). System identification for FES-based tremor suppression. *European Journal of Control*, 27, 45–59.
- Donkers, T., van de Wijdeven, J., & Bosgra, O. (2008). Robustness against model uncertainties of norm optimal iterative learning control. In *2008 American control conference* (pp. 4561–4566).
- Excell, T., Freeman, C. T., Meadmore, K., et al. (2013). Optimisation of hand posture stimulation using an electrode array and iterative learning control. *Journal of Automatic Control*, 21(1), 1–4.
- Freeman, C. T. (2016). Control system design for electrical stimulation in upper limb rehabilitation. In *Springer international publishing*, (pp. 1–2). Springer International Publishing.
- Freeman, C. T., & French, M. (2015). Estimation based multiple model iterative learning control. In *2015 54th IEEE conference on decision and control* (pp. 6070–6075).
- Freeman, C. T., Hughes, A. M., Burridge, J. H., Chappell, P. H., Lewin, P. L., & Rogers, E. (2009). A model of the upper extremity using FES for stroke rehabilitation. *Journal of Biomechanical Engineering*, 131(3).
- Freeman, C. T., Lewin, P. L., & Rogers, E. (2005). Experimental evaluation of iterative learning control algorithms for non-minimum phase plants. *International Journal of Control*, 78(11), 826–846.
- Freeman, C. T., Lewin, P. L., Rogers, E., et al. (2009). Discrete Fourier transform based iterative learning control design for linear plants with experimental verification. *Journal of Dynamic Systems, Measurement, and Control*, 131(3), Article 031006–1–031006–10.
- Geller, D., Goldberg, C., Winterbottom, L., Nilsen, D. M., Mahoney, D., & Gillen, G. (2023). Task-oriented training with cognitive strategies for adults with stroke to improve ADL and/or functional mobility performance (2012–2019). *American Journal of Occupational Therapy*, 77(1), Article 7710393030.

- Gföhler, M., Angeli, T., & Lugner, P. (2004). Modeling of artificially activated muscle and application to fcs cycling. *Journal of Mechanics in Medicine and Biology*, 04(01), 77–92.
- Hodkin, E. F., Lei, Y., Humby, J., Glover, I. S., Choudhury, S., Kumar, H., et al. (2018). Automated FES for upper limb rehabilitation following stroke and spinal cord injury. *IEEE Transactions on Neural Systems and Rehabilitation Engineering*, 26(5), 1067–1074.
- Klauer, C., Ambrosini, E., Ferrante, S., et al. (2019). Co-activation and eEMG-feedback for restoring hand-functions. In *2019 18th European control conference* (pp. 191–196).
- Kristensen, M. G. H., Busk, H., & Wienecke, T. (2022). Neuromuscular electrical stimulation improves activities of daily living post stroke: A systematic review and meta-analysis. *Journal of Electromyography and Kinesiology*, 4(1), Article 100167.
- Kutlu, M., Freeman, C. T., Hallewell, E., et al. (2016). Upper-limb stroke rehabilitation using electrode-array based functional electrical stimulation with sensing and control innovations. *Medical Engineering & Physics*, 38(4), 366–379.
- Le, F., Markovskiy, I., Freeman, C. T., & Rogers, E. (2010). Identification of electrically stimulated muscle models of stroke patients. *Control Engineering Practice*, 18(4), 396–407.
- Lee, J. H., Lee, K. S., & Kim, W. C. (2000). Model-based iterative learning control with a quadratic criterion for time-varying linear systems. *Automatica*, 36(5), 641–657.
- Li, X., Wang, K., & Liu, D. (2014). An improved result of multiple model iterative learning control. *IEEE/CAA Journal of Automatica Sinica*, 1(3), 315–322.
- Li, X., & Zhang, W. (2010). Multiple model iterative learning control. *Neurocomputing*, 73(13), 2439–2445.
- Liu, Y., Qin, Y., Huo, B., & Wu, Z. (2020). Functional electrical stimulation based bicep force control via active disturbance rejection control. In *2020 5th international conference on advanced robotics and mechatronics* (pp. 306–311).
- Longman, R., Peng, Y., Kwon, T., et al. (2011). Adaptive inverse iterative learning control. *Journal of the Chinese Society of Mechanical Engineers, Transactions of the Chinese Institute of Engineers - Series C*, 32(6), 493–506.
- Ma, L., Liu, X., Kong, X., & Lee, K. Y. (2021). Iterative learning model predictive control based on iterative data-driven modeling. *IEEE Transactions on Neural Networks and Learning Systems*, 32(8), 3377–3390.
- Meng, D. (2019). Convergence conditions for solving robust iterative learning control problems under nonrepetitive model uncertainties. *IEEE Transactions on Neural Networks and Learning Systems*, 30(6), 1908–1919.
- Meng, D., & Moore, K. L. (2017). Robust iterative learning control for nonrepetitive uncertain systems. *IEEE Transactions on Automatic Control*, 62(2), 907–913.
- Nahrstaedt, H., Schauer, T., Shalaby, R., Hesse, S., & Raisch, J. (2008). Automatic control of a drop-foot stimulator based on angle measurement using bioimpedance. *Artificial Organs*, 32(8), 649–654.
- Oliveira, T. R., Costa, L. R., Catunda, J. M. Y., et al. (2017). Time-scaling based sliding mode control for neuromuscular electrical stimulation under uncertain relative degrees. *Medical Engineering & Physics*, 44, 53–62.
- Owens, D. H. (2016). *Iterative learning control: An optimization paradigm (Advances in industrial control)*. New York: Springer.
- Owens, D. H., Freeman, C. T., & Chu, B. (2014). An inverse-model approach to multivariable norm optimal iterative learning control with auxiliary optimisation. *International Journal of Control*, 87(8), 1646–1671.
- Padmanabhan, R., Bhushan, M., Hebbar, K. K., et al. (2021). Second-level adaptation and optimization for multiple model adaptive iterative learning control. In *2021 seventh Indian control conference* (pp. 289–294).
- Party, L. I. S. W. (2023). National clinical guideline for stroke for the UK and Ireland. Available at www.strokeguideline.org.
- Pelton, T., van Vliet, P., & Hollands, K. (2012). Interventions for improving coordination of reach to grasp following stroke: A systematic review. *International Journal of Evidence-Based Healthcare*, 10(2), 89–102.
- Popović, D. B. (2014). Advances in functional electrical stimulation (FES). *Journal of Electromyography and Kinesiology*, 24(6), 795–802.
- Ratcliffe, J. D., Hatonen, J. J., Lewin, P. L., Rogers, E., Harte, T. J., & Owens, D. H. (2005). P-type iterative learning control for systems that contain resonance. *International Journal of Adaptive Control and Signal Processing*, 19(10), 769–796.
- Ratcliffe, J. D., Lewin, P. L., Rogers, E., Hatonen, J. J., & Owens, D. H. (2006). Norm-optimal iterative learning control applied to gantry robots for automation applications. *IEEE Transactions on Robotics*, 22(6), 1303–1307.
- Razavian, R. S., Ghannadi, B., Mehrabi, N., et al. (2018). Feedback control of functional electrical stimulation for 2-D arm reaching movements. *IEEE Transactions on Neural Systems and Rehabilitation Engineering*, 26(10), 2033–2043.
- Resquín, F., Cuesta Gómez, A., Gonzalez-Vargas, J., Brunetti, F., Torricelli, D., Molina Rueda, F., et al. (2016). Hybrid robotic systems for upper limb rehabilitation after stroke: A review. *Medical Engineering & Physics*, 38(11), 1279–1288.
- Resquín, F., Gonzalez-Vargas, J., nez, J. I., et al. (2016). Feedback error learning controller for functional electrical stimulation assistance in a hybrid robotic system for reaching rehabilitation. *European Journal of Translational Myology*, 26(3), 255–261.
- Rogers, E., Chu, B., Freeman, C., & Lewin, P. (2023). *Iterative learning control algorithms and experimental benchmarking*. Wiley, New York.
- Rouhani, H., Popovic, M. R., Same, M., Li, Y. Q., & Masani, K. (2016). Identification of ankle plantar-flexors dynamics in response to electrical stimulation. *Medical Engineering & Physics*, 38(11), 1166–1171.
- Rouse, C. A., Parikh, A., Duenas, V., et al. (2016). Compensating for changing muscle geometry of the biceps brachii during neuromuscular electrical stimulation: A switched systems approach. In *2016 IEEE 55th conference on decision and control* (pp. 1328–1333).
- Sa-e, S., Freeman, C. T., & Yang, K. (2020). Iterative learning control of functional electrical stimulation in the presence of voluntary user effort. *Control Engineering Practice*, 96, Article 104303.
- Sampson, P., Freeman, C., Coote, S., Demain, S., Feys, P., Meadmore, K., et al. (2016). Using functional electrical stimulation mediated by iterative learning control and robotics to improve arm movement for people with multiple sclerosis. *IEEE Transactions on Neural Systems and Rehabilitation Engineering*, 24(2), 235–248. <http://dx.doi.org/10.1109/TNSRE.2015.2413906>.
- Schauer, T. (2017). Sensing motion and muscle activity for feedback control of functional electrical stimulation: Ten years of experience in Berlin. *Annual Reviews in Control*, 44, 355–374.
- Scheerer, E. M., Liao, Y.-W., Perreault, E. J., Tresch, M. C., Memberg, W. D., Kirsch, R. F., et al. (2012). System identification for 3D force control of a human arm neuroprosthesis using functional electrical stimulation. In *2012 IEEE international conference on robotics and automation* (pp. 3698–3705).
- Sharma, N., Gregory, C. M., & Dixon, W. E. (2011). Predictor-based compensation for electromechanical delay during neuromuscular electrical stimulation. *IEEE Transactions on Neural Systems and Rehabilitation Engineering*, 19(6), 601–611.
- Sun, Z., Qiu, T., Iyer, A., Dicianno, B. E., & Sharma, N. (2023). Continuous switching control of an input-delayed antagonistic muscle pair during functional electrical stimulation. *IEEE Transactions on Control Systems Technology*, 31(1), 306–316.
- Tan, H. G., Shee, C. Y., Kong, K. H., Guan, C., & Ang, W. T. (2011). EEG controlled neuromuscular electrical stimulation of the upper limb for stroke patients. *Frontiers of Mechanical Engineering*, 6(1), 71–81.
- Turk, R., Notley, S. V., Pickering, R. M., Simpson, D. M., Wright, P. A., & Burridge, J. H. (2008). Reliability and sensitivity of a wrist rig to measure motor control and spasticity in post-stroke hemiplegia. *Neurorehabilitation and Neural Repair*, 22(6), 684–696.
- Westerveld, A. J., Schouten, A. C., Veltink, P. H., & van der Kooij, H. (2014). Passive reach and grasp with functional electrical stimulation and robotic arm support. In *2014 36th annual international conference of the IEEE engineering in medicine and biology society* (pp. 3085–3089).
- Wiarta, S. S., Arifin, A., Baki, S. H., Arrofiqi, F., Fatoni, M. H., & Watanabe, T. (2020). Design of post-stroke upper limb rehabilitation game using functional electrical stimulation for hemiplegic patient. In *2020 international conference on computer engineering, network, and intelligent multimedia* (pp. 6–11).
- Willems, J. C. (2004). Deterministic least squares filtering. *Journal of Econometrics*, 118(1–2), 341–373.
- Wolf, D. N., Hall, Z. A., & Scheerer, E. M. (2020). Model learning for control of a paralyzed human arm with functional electrical stimulation. In *2020 IEEE international conference on robotics and automation* (pp. 10148–10154).
- Wolf, D. N., & Scheerer, E. M. (2017). Evaluating an open-loop functional electrical stimulation controller for holding the shoulder and elbow configuration of a paralyzed arm. In *2017 international conference on rehabilitation robotics* (pp. 789–794).
- Wolf, D. N., & Scheerer, E. M. (2018). Holding static arm configurations with functional electrical stimulation: A case study. *IEEE Transactions on Neural Systems and Rehabilitation Engineering*, 26(10), 2044–2052.
- Wolf, D. N., & Scheerer, E. M. (2019). Simple quasi-static control of functional electrical stimulation-driven reaching motions. In *2019 9th international IEEE/eMBS conference on neural engineering* (pp. 211–214).
- Wolf, D. N., & Scheerer, E. M. (2022). Trajectory optimization and model predictive control for functional electrical stimulation-controlled reaching. *IEEE Robotics and Automation Letters*, 7(2), 3093–3098.
- Wu, Q., Wang, X., Du, F., et al. (2017). Modeling and position control of a therapeutic exoskeleton targeting upper extremity rehabilitation. *Proceedings of the Institution of Mechanical Engineers, Part C (Mechanical Engineering Science)*, 231(23), 4360–4373.
- Xu, J., & Xu, J.-X. (2013). Iterative learning control for output-constrained systems with both parametric and nonparametric uncertainties. *Automatica*, 49(8), 2508–2516.
- Zames, G., & El-sakkary, A. K. (1980). Unstable systems and feedback: The gap metric. In *Roc. of the allerton conference* (pp. 380–385).
- Zhang, Z., Chu, B., Liu, Y., et al. (2020). FES-based wrist tremor suppression using multi-periodic repetitive control. *IFAC-PapersOnLine*, 53(2), 10135–10140.
- Zhang, F., Meng, D., & Cai, K. (2023). Safe iterative learning for attitude tracking of rigid bodies under nonconvex constraints. *IEEE Transactions on Automation Science and Engineering*, 1–13.
- Zhou, J., Freeman, C. T., & Holderbaum, W. (2023a). Multiple model iterative learning control for FES-based stroke rehabilitation. In *2023 American control conference* (pp. 2147–2152).
- Zhou, J., Freeman, C. T., & Holderbaum, W. (2023b). Multiple model iterative learning control with application to upper limb stroke rehabilitation. In *2023 international interdisciplinary PhD workshop* (pp. 1–6).
- Zhu, Q., Xu, J., Huang, D., et al. (2015). Iterative learning control design for linear discrete-time systems with multiple high-order internal models. *Automatica*, 62, 65–76.